Draft version January 30, 2019
Typeset using LaTeX **twocolumn** style in AASTeX62

Short Term Variability of Evolved Massive Stars with TESS

Trevor Z. Dorn-Wallenstein,[1] Emily M. Levesque,[1] and James R. A. Davenport[2,*]

[1] *University of Washington Astronomy Department*
Physics and Astronomy Building, 3910 15th Ave NE
Seattle, WA 98105, USA
[2] *University of Washington Astronomy Department*
Physics and Astronomy Building, 3910 15th Ave NE
Seattle9, WA 98105, USA

(Received; Revised; Accepted)

Submitted to ApJL

ABSTRACT

We present the first results from a study of TESS Sector 1 and 2 light curves for seven evolved massive stars in the LMC: five yellow supergiants (YSGs) and two luminous blue variables (LBVs), including S Doradus. We find coherent short-timescale variability in both LBVs and three of the YSGs. One of the YSGs, HD 269953, displays drastically different variability from its fellows, which may indicate nonradial pulsations. While the field surrounding HD 269953 is quite crowded, it is the brightest star in the region, and has infrared colors indicating it is dusty. We suggest HD 269953 may be in a post-red supergiant evolutionary phase. We find a signal with a period of ~ 5 days for the LBV HD 269582. The periodogram of S Doradus shows a complicated structure, with peaks below frequencies of 1.5 cycles per day. We analyze the noise characteristics of all seven light curves, and find a red noise component in all of them. However, the power law slope of the red noise and the timescale over which coherent structures arise changes from star to star. Our results highlight the potential for studying evolved massive stars with TESS.

Keywords: stars: massive, stars: evolution, stars: oscillations, stars: rotation, stars: variables: general

1. INTRODUCTION

The environments in and around evolved massive stars are complex and unique astrophysical laboratories. Much of the information about the physics of these stars is encoded within their variability. However, due to their rarity, the behavior of massive stars in the time domain is still poorly studied by high-precision space-based instruments. Thus, the critical physical ingredients that inform our models of evolved massive stars (e.g., the distribution of rotation rates, asteroseismically determined masses and radii, short-timescale wind-driven variability and more) are still poorly constrained by observations.

Corresponding author: Trevor Z. Dorn-Wallenstein
tzdw@uw.edu

* DIRAC Fellow

On the main sequence, massive stars manifest themselves as O and B dwarfs earlier than spectral type ∼B3 (Habets & Heintze 1981). During and shortly after the main sequence phase, mass loss rates are at their lowest (Puls et al. 2008; Smith 2014), and the geometries of their circumstellar media (CSM) are at their simplest (e.g., Garcia-Segura et al. 1996; Gvaramadze et al. 2018). Thus, rotational modulation from bright spots on the stellar surface (e.g., Ramiaramanantsoa et al. 2018) or Co-rotating Interaction Regions (CIRs, see Mullan 1984; Cranmer & Owocki 1996) in the stellar wind can be readily observed by *CoRoT*, *Kepler*, and K2 (see Blomme et al. 2011; Buysschaert et al. 2015; Balona et al. 2015; Balona 2016; Johnston et al. 2017, and more).

At shorter ($\lesssim$hour) timescales, asteroseismic oscillations in B (and more recently O) stars have been detected (e.g., Balona et al. 2011; Blomme et al. 2011;

Buysschaert et al. 2015; Johnston et al. 2017) as p-modes in β Cephei pulsators, g-modes in Slowly Pulsating B-type (SPB) stars, or a combination of both (Daszynska-Daszkiewicz et al. 2018). Finally, there are sources of stochastic or noncoherent variability (Blomme et al. 2011) that could arise due to the sub-surface convection zone (which may interact with asteroseismic pulsations, see Perdang 2009), granulation, or inhomogeneities in the stellar wind. Additional white noise may manifest itself at ∼hour timescales due to instabilities in the stellar wind (Krtička & Feldmeier 2018).

Beyond the OB phases, however, massive stars are poorly understood at short timescales. No post-main-sequence massive stars were observed by *Kepler* or K2, and only small samples of evolved stars at specific evolutionary phases were have been observed with targeted campaigns using *CoRoT* or the BRITE constellation. That said, post-main-sequence massive stars are fantastic targets for high cadence photometry. In red supergiants (RSGs), convective and pulsational processes can generate variability on long timescales (Wood et al. 1983), which helps RSGs launch dusty stellar winds (Yoon & Cantiello 2010, and references therein). Simulations of red supergiants (Chiavassa et al. 2011) predict large scale convective motions, turbulence, and shocks, all of which can manifest themselves coherently or stochastically (e.g., red noise detected in AAVSO light curves of RSGs by Kiss et al. 2006).

Studies of photometric variability in Wolf-Rayet stars are still relatively few in number. The BRITE constellation has studied six of the brightest Wolf-Rayet stars (Moffat et al. 2018), and detected CIRs, binary interactions, and stochastic variability. However, with such a small sample size, little can be said about how the variability of Wolf-Rayets depends on fundamental stellar parameters like temperature and luminosity. Finally, stars in transitional states with lifetimes of only a few 10^4 years (e.g., Yellow Supergiants, luminous blue variables, "slash" stars, etc.) have gone completely unobserved, due to their rarity and thus their lack of concentration on the sky; any pointing by a mission with a stationary field of view (e.g., *Kepler*) isn't likely to include many short-lived evolutionary phases of massive stars. However, many of these evolutionary phases are still poorly understood. Many of them are associated with dusty circumstellar mediums, outbursts, and other phenomena. Their pulsational or rotational properties can be used to infer information about their interior states and evolution, including angular momentum transport, convection, surface differential rotation and more.

The Transiting Exoplanet Survey Satellite (TESS) is a nearly all-sky photometry mission targeting ∼20,000 bright stars per year at a two-minute cadence (with full-frame images for ∼20 million stars every thirty minutes), yielding approximately 27 days of continuous photometry for stars close to the ecliptic plane, with longer light curves for stars observed by multiple spacecraft pointings. Large numbers of evolved massive stars in the Galaxy and the Magellanic Clouds are bright enough to be observed by TESS over the course of its nominal two-year mission. Here we present analysis of the first evolved massive star light curves to become available from TESS sectors 1 and 2. In §2, we discuss our sample selection using data from the *Gaia* mission. Results for each star are presented in §3. We discuss the relevance of our findings for stellar evolution theory, and the prospects of a dedicated TESS campaign to observe evolved massive stars in §4, before concluding in §5

2. SAMPLE SELECTION AND DATA CLEANING

Our sample relies upon the accurate astrometry published in the second data release (DR2) of the *Gaia* (Gaia Collaboration et al. 2018), which contains position and brightness measurements in the broad *Gaia* passband G for 1.7 billion stars, of which 1.4 billion have photometry in the blue and red bandpasses G_{BP} and G_{RP}, and 1.3 billion have parallax ϖ and proper motion μ measurements. We acquired the TESS Sectors 1 and 2 target lists[1], uploaded them to the ESA *Gaia* archive[2], and searched for objects in *Gaia* DR2 and the TESS target lists that were separated by less than 1".

In theory, *Gaia* parallaxes are easily convertible to distances via

$$\frac{d}{\mathrm{pc}} = \frac{\mathrm{arcsec}}{\varpi} \tag{1}$$

which would allow for a direct measurement of luminosity, and then used to select massive stars. However, converting from parallax to distance is a nontrivial task in practice. Systematics — e.g., parallax and proper motion zero-point offsets measured from distant QSOs — exist in the data (Lindegren et al. 2018), and many objects have high fractional errors (σ_ϖ/ϖ) or negative measured parallax. In a Bayesian framework these measurements are all useful, and Bailer-Jones et al. (2018) inferred distances for the majority of stars in *Gaia* DR2 accounting for these effects, using a prior based on the spatial distribution of stars in the galaxy. For stars in

[1] Target lists obtainable at https://tess.mit.edu/observations/sector-1/ and https://tess.mit.edu/observations/sector-2/ respectively

[2] https://gea.esac.esa.int/archive/

the TESS–*Gaia* cross-match, we calculated the absolute G magnitude:

$$M_G = G - 5\log_{10} r_{est} + 5 - A_G \quad (2)$$

using the estimated distance r_{est} from Bailer-Jones et al. (2018), and the published estimate of the extinction A_G. We also estimated the reddening as

$$E(G_{BP} - G_{RP}) = \frac{A_G}{A_G/A_V}\left(\frac{A_{BP}}{A_V} - \frac{A_{RP}}{A_V}\right) \quad (3)$$

using the estimated extinction A_G, and coefficients from Malhan et al. (2018). We make the cross-matched data, as well as the estimated M_G and $G_{BP} - G_{RP}$ publicly available online.[3]

For stars without an estimated A_G, we also estimate a lower limit to the absolute magnitude

$$M_G \leq G - 5\log_{10} r_{est} + 5 \quad (4)$$

and an upper limit to the intrinsic $G_{BP} - G_{RP}$ by assuming $E(G_{BP} - G_{RP}) = 0$. We can then construct accurate color-magnitude diagrams (CMDs), which we can use to select massive stars from targets observed by TESS. We use isochrones from the MESA Isochrones & Stellar Tracks (MIST, Dotter 2016; Choi et al. 2016) group, which adopts stellar models from the Modules for Experiments in Stellar Astrophysics (MESA, Paxton et al. 2011, 2013, 2015) code. In particular we chose isochrones with metallicity $[Fe/H] = 0.25$, and rotation speed relative to critical of $v/v_{crit} = 0.4$. We then selected the faintest isochrone point with initial mass $M_i \geq 8$ M$_\odot$ in small bins of $G_{BP} - G_{RP}$, forming a boundary in color-magnitude space above which a star is likely to be massive — note that many isochrone points with $M_i < 8$ M$_\odot$ lie above this boundary, so our sample is not constructed to be free of contamination. We show this boundary, as well as *Gaia* colors and absolute magnitudes in Figure 1. Points in blue are stars for which our estimate of M_G and $G_{BP} - G_{RP}$ include the extinction, and stars in orange are those without estimates of A_G in *Gaia* DR2. The black line denotes our luminosity cutoff for selecting massive stars.

Of these stars, many are galactic long period variables (LPVs), and a number are main sequence or giant OB stars, as well as some Be stars, and all were observed for specific OB or Be asteroseismology programs (Pedersen et al. 2019). Unsurprisingly, most of the remaining evolved massive stars were all in the LMC. Since Bailer-Jones et al. (2018) used a galactic stellar distribution model as a prior when estimating distances, the distances to known LMC stars are systematically too close, and thus their luminosities are *underestimated*. However, the stars that we do select are the most luminous stars observed in the LMC, and thus the stars least affected by crowding issues, which can be significant for TESS's 21" pixels[4].

To ensure we did not miss any interesting evolved massive stars, we also cross-matched the spectroscopically studied LMC stars from Table 4 of Massey (2002) with our TESS/*Gaia* cross-match, assumed an average $E(B-V) = 0.13$ towards the LMC (Massey et al. 2007), a total-to-selective extinction ratio $R_V = 3.41$ (Gordon et al. 2003), and coefficients from Malhan et al. (2018) to calculate the average A_G and $E(G_{BP}-G_{RP})$ towards the LMC. Using these values, and a distance modulus for the LMC of $\mu = 18.52$ (Kovács 2000), we selected an additional 19 LMC stars, all of which were main sequence or supergiant OB stars, which we choose not to study in lieu of more focused work by other teams. This leaves us with a total of seven evolved massive stars in Sectors 1 and 2 observed at two-minute cadence with TESS. We list the evolutionary stage, T magnitude and ID number from the TESS Input Catalog (TIC, Stassun et al. 2018), 2MASS J magnitude (Cutri et al. 2003), and 2MASS/IRAC colors using data from Bonanos et al. (2009) in Table 1[5].

We show the results of our sample selection in the *Gaia* color-magnitude diagram in Figure 1. Points in blue are stars for which our estimate of M_G and $G_{BP} - G_{RP}$ include the extinction, and stars in orange are those without estimates of A_G in *Gaia* DR2. Green points are stars from Massey (2002). The black line denotes our luminosity cutoff for selecting massive stars. Points outlined in grey boxes are either low mass AGB LPVs or relatively unevolved O and B stars that we ignore for this study. The seven evolved massive stars that we select for this study are highlighted in red.

2.1. *Data Cleaning*

The TESS team released raw light curves and full-frame images from Sectors 1 and 2 on 6 December

[3] https://github.com/tzdwi/TESS-Gaia

[4] One evolved supergiant, HD 269902, is in the incredibly-crowded 30 Doradus starburst region. Due to the large number of bright targets located within a single 21" TESS pixel around HD 269902, we choose not to analyze this star. Additionally we the F0 subgiant HD 210767 was selected, which has a large *Gaia* DR2 proper motion. It may be that HD 210767 is indeed an evolved massive star; without a spectroscopic confirmation, we also chose not to study it.

[5] As an aside: the fact that all seven of these stars are in the LMC emphasizes the need for TESS programs targeting galactic evolved massive stars, where the targets are brighter and less crowded.

Table 1. TESS two-minute cadence targets. TIC # and T magnitude are from the TIC; J magnitude is from 2MASS (Cutri et al. 2003), and 3.6, 4.5, 5.8, and 8.0 μm magnitudes are from the Spitzer SAGE LMC survey (Bonanos et al. 2009).

Common Name	Evolutionary Stage	TIC #	T	J	$J-[3.6]$	$J-[4.5]$	$J-[5.8]$	$J-[8.0]$
			[mag]	[mag]	[mag]	[mag]	[mag]	[mag]
S Dor	LBV	179305185	9.16	8.683	0.923	1.036	1.164	1.373
HD 269953	YSG	404850274	9.22	8.588	1.311	1.89	2.363	3.427
HD 269582	Ofpe/WN9 → LBV	279957111	9.33	12.041	2.814	3.188	3.255	3.612
HD 270046	YSG	389437365	9.45	8.713	0.712	0.748	0.933	0.894
HD 270111	YSG	389565293	9.63	9.073	0.535	0.578	0.599	0.480
HD 269110	YSG	40404470	10.01	9.320	0.560	0.643	0.695	0.891
HD 268687	YSG	29984014	10.21	9.693	0.397	0.523	0.608	0.706

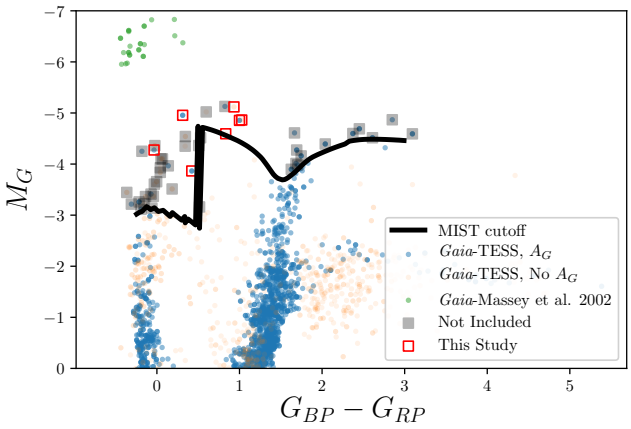

Figure 1. *Gaia* CMD for TESS Sector 1 and 2 targets. Stars with an estimate of A_G are in blue, while stars without an A_G estimate are in orange; for these stars, colors are upper limits, and magnitudes are lower limits. The black line represents our minimum-luminosity criteria to select massive stars. Stars in grey boxes are either low mass stars, or relatively unevolved O and B stars. Green points are O and B supergiants from Massey (2002). The red boxes indicate the seven evolved massive stars we select for this study.

2018. We downloaded all light curves from The Mikulski Archive for Space Telescopes (MAST), and selected the light curves associated with the TIC numbers of our targets. Because these light curves are processed by the first iteration of the TESS pipeline, we err on the side of caution, assuming that the raw light curves contain numerous instrumental effects. Thus we select only those points with the `QUALITY` flag set to 0. We then normalize the light curves by dividing the raw `PDCSAP_FLUX` by the median. For targets observed in both Sectors 1 and 2, we choose to median-divide each Sector individually before concatenating the light curves. While this helps to eliminate Sector-to-Sector offsets and systematics, it can also erase variations at timescales longer than ∼1 month. We plot all of the normalized light curves, along with a rolling 128-point median in orange, in Figure 2. Finally, for stars with obvious longer-term trends that would mask otherwise interesting behavior, (e.g., the increase in flux at the beginning of the light curve for HD 268687), we fit the light curve with a low-order polynomial, and normalize the data by the fit, which effectively acts as a low-pass filter in the Fourier domain.

3. RESULTS

3.1. *Yellow Supergiants*

From the Geneva evolutionary tracks (Ekström et al. 2012), a 25 $M_\odot$ solar-metallicity star begins its life as an O6 dwarf. After 7 Myr, it has evolved into a B0 supergiant, at which point it crosses the HR diagram in under a Myr to become a RSG. Approximately 500 kyr later, it has evolved bluewards once more to become a Wolf-Rayet star (Massey et al. 2017). During both rightward and leftward crossings of the HR diagram, the star undergoes an incredibly brief yellow supergiant (YSG) phase. Thus, while the luminosities and effective temperatures of two given YSGs may be identical, their initial masses, ages, and interior structures may be radically different. Signatures of these differences may be imprinted in the TESS lightcurves. While it is likely that a cool YSG that has previously undergone a RSG phase will be accompanied by a dusty envelope, as the star's effective temperature increases, the dust may be photodissociated, which is consistent with the decreasing abundance of circumstellar dust species around increasingly hot evolved massive stars in Table 1 of Waters (2010). Therefore, it is possible that variability may be the best or most unambiguous means of distinguishing between rightward- and leftward-moving YSGs Finding leftward-moving YSGs places a valuable upper limit on the initial masses of stars that explode

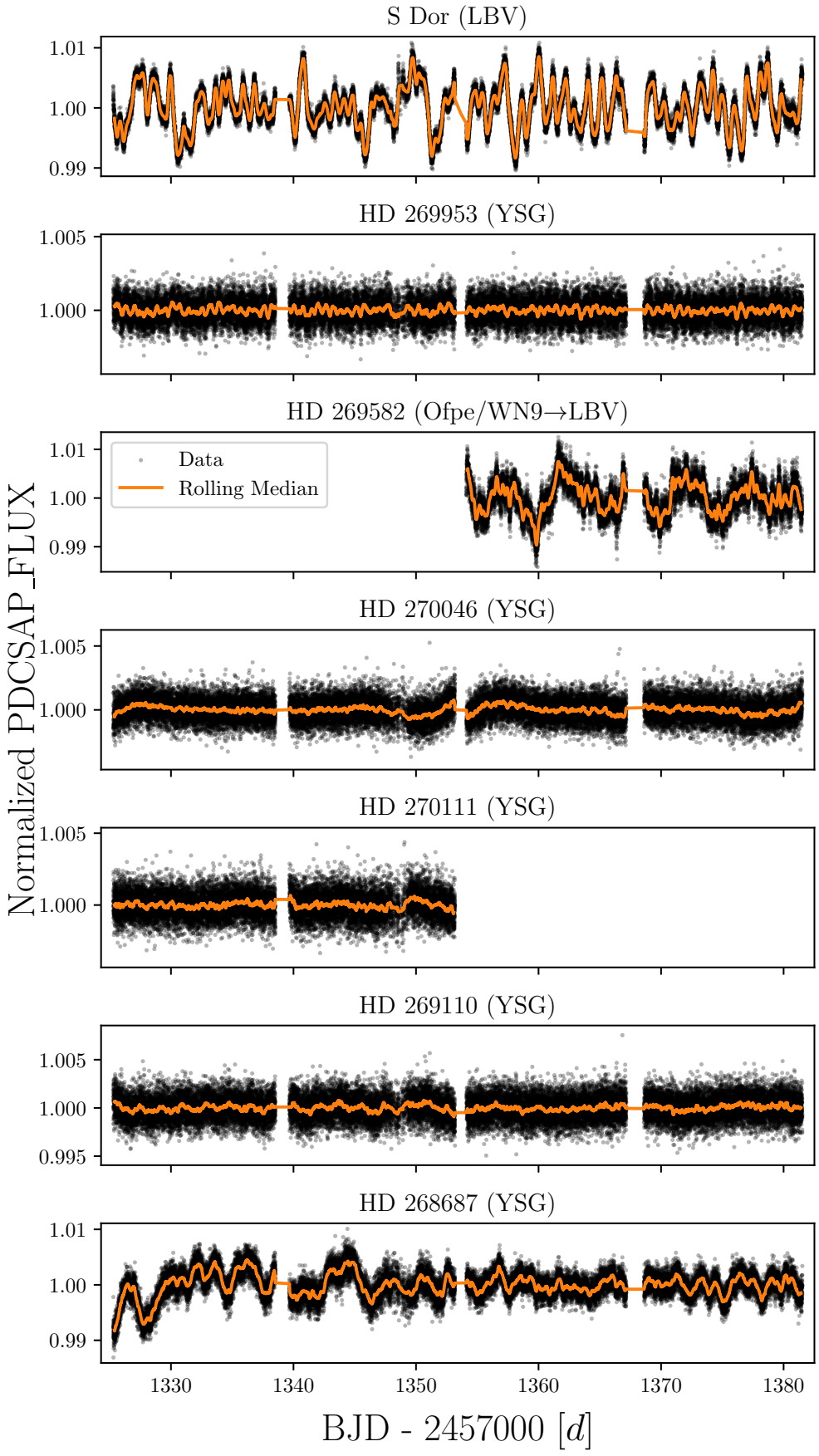

Figure 2. Normalized TESS light curves for the seven target stars. Data are in black points, and a rolling 128-point median is plotted in orange.

as RSGs before they can become YSGs (a.k.a., "the red supergiant problem", e.g., Smartt et al. 2009).

3.1.1. *HD 269953*

HD 269953 is a G0 YSG, assigned a luminosity class of 0 by Keenan & McNeil (1989), which is in agreement with its high luminosity $\log(L/L_\odot) = 5.437$ from Neugent et al. (2012). Coupled with its temperature $T_{eff} = 4920$ K, this implies a radius of 566 $R_\odot$ from the Stephan-Boltzmann law. While the light curve presented in Figure 2 appears to be dominated by noise, the light curve smoothed by a 128-point rolling median appears to show coherent oscillations. We re-plot the smoothed, mean-subtracted light curve in the top panel of Figure 3. We use Astropy (Astropy Collaboration et al. 2013; The Astropy Collaboration et al. 2018) to calculate the Lomb-Scargle Periodogram (Lomb 1976; Scargle 1982) on the unsmoothed data for frequencies between 1/28 and 5 days^{-1}, which shows a strong peak at 1.59 day^{-1}, as well as its harmonics (indicated by the red vertical lines), and several other lower-amplitude peaks. Of the better-resolved peaks at high frequencies, many of them are surrounded by less significant peaks that could be asteroseismic in origin.

With high amounts of IR reddening, HD 269953 is the dustiest YSG in our sample, making it quite likely that it is in a post-RSG phase. Thus, a direct measurement of its mass via asteroseismology would be an incredibly valuable constraint on stellar evolution. Unfortunately, it is located in the star-forming LMC cluster NGC 2085, and thus is subject to a high degree of crowding in TESS's 21" pixels. While HD 269953 is the brightest star by far in the field, we reserve further analysis of the light curve until more advanced tools are developed to extract light curves from crowded regions in TESS. Regardless, it is readily apparent that the periodogram of HD 269953 is drastically different from the periodograms of the two other YSGs discussed below. This, coupled with its apparently more-evolved state, suggests a distinct difference in variability between pre- and post-RSG warm supergiants.

3.1.2. *HD 269110 & HD 268687*

HD 269110 is a lower luminosity YSG with $\log(L/L_\odot) = 5.251$, $T_{eff} = 5624$ K (Neugent et al. 2012), and thus a radius of 445 $R_\odot$. It has a spectral type of G0I from Ardeberg et al. (1972). Similar to HD 269954, the light curve presented in Figure 2 appears to be just noise, while the light curve smoothed by a 128-point rolling median shows coherent variability at approximately 750 ppm. Figure 4 shows the smoothed, mean-subtracted light curve in the top panel, and the periodogram in the bottom. The periodogram shows a strong peak at 0.55 day^{-1} (a period of 1.81 days), with one harmonic easily visible, as well as a group of peaks centered at $\nu_{max} = 0.115$ day^{-1} with an average frequency spacing $\Delta\nu = 0.032$ day^{-1}. Application of the standard solar asteroseismic scaling relations from Kjeldsen & Bedding (1995) yields a mass of ~ 1.4 $M_\odot$. Since we are extrapolating from a solar model, this highlights the need for improved asteroseismic models for high mass stars with drastically different structures physics than the sun.

HD 268687 is classified as a F6Ia supergiant by Ardeberg et al. (1972), and has a luminosity $\log(L/L_\odot) = 5.169$ and effective temperature $T_{eff} = 6081$ K from Neugent et al. (2012), implying a radius of 346 $R_\odot$. After normalizing the light curve by a 7th-order polynomial fit, we calculate the periodogram for frequencies between 1/30 and 2 day^{-1}, which we plot in Figure 5. The periodogram shows a clear peak at 0.339 day^{-1}, corresponding to a period of 2.95 days, which is readily visible in the light curve. We indicate this frequency and its first four harmonics with vertical red lines. The periodogram also shows a broad bump of peaks accompanying the dominant peak at lower frequencies, and a number of less signifcant peaks at higher frequencies.

All told, both YSGs are in similar physical sates, and both show clear peaks in their periodograms on timescales of 2-3 days, in addition to complex structure at higher frequencies. We can rule out some possible sources of this variability. If both stars are approximately 25 $M_\odot$ and the variability is due to binary interactions with a companion, the companion would have to be approximately 64,000 $M_\odot$ to be in a 2.95-day Keplerian orbit outside of the stellar surface of HD 268687, and 360,000 $M_\odot$ to be in a 1.81-day Keplerian orbit around HD 269110. We determine both scenarios to be highly implausible.

Perhaps the brightness modulations are instead due to one or more spots on the surface of the stars, causing the apparent luminosity to change as the star rotates? If the typical spot latitude were at the stellar equator, then the star would be rotating at approximately 6,000 km s^{-1} for HD 268687, and 12,000 km s^{-1} for HD 269110, well beyond the critical velocity for both stars. However, we cannot rule out a nearly-polar spot. This option is somewhat attractive given the change in the shape of the variability in HD 268687 with time, but would require invoking severe surface differential rotation, as well as extremely fast spot decay times to explain the change of the variability in HD 269110.

The final possibility, which is also consistent with the change in the shape of the variability, is that we are observing coherent asteroseismic variability in in both stars, in addition to the apparent "frequency comb" seen

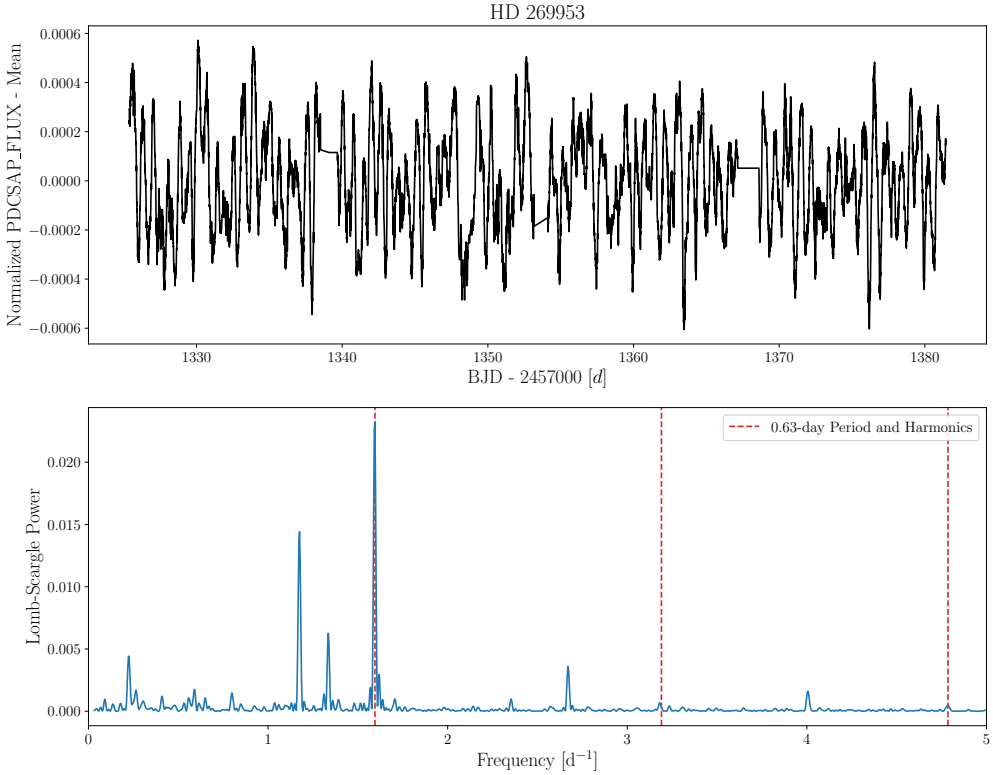

Figure 3. *Top*: Light curve for HD 269953, after smoothing with a 128-point rolling median, showing coherent variability at approximately 600 ppm. *Bottom*: Lomb-Scargle Periodogram, calculated for frequencies between 1/30 and 5 day^{-1}. The strongest peak and its harmonics are indicated with red vertical lines.

in the periodogram of HD 269110. YSGs have been observed to vary with periods of many tens of days (Arellano Ferro 1985) caused by He ionization-driven radial pulsations. Perhaps we are observing a very high-order harmonic of a radial mode. Alternately, oscillations in a non-radial mode may be causing this variability. Because both stars are in the LMC, it, and most of our other targets, are in the TESS Continuous Viewing Zone (CVZ), and will be observed almost continuously for a year. If these oscillations are p- or g-mode pulsations, some of the peaks in the periodogram may resolve into additional frequency combs characteristic of these pulsations. Another option is that the variability is caused by Rossby waves (or r-mode oscillations, Papaloizou & Pringle 1978), which appear as "hump and spike" shapes in the periodogram (Saio et al. 2018), which have been observed in main sequence F and G stars. While the fundamental mode is located at a slightly lower frequency than the rotational frequency (and hence we run into the same problems as above), higher-azimuthal-order frequencies can arise. Unfortunately the amplitude of the oscillations declines sharply at the higher orders, implying that the rotation speeds would only be a factor of a few slower, which is still physically implausible.

3.1.3. *Noise Properties of YSG Light Curves*

In addition to the peaks in periodograms of the three YSGs discussed above, all five YSGs display rising power at lower frequencies (i.e., red noise). Red noise is seemingly ubiquitous in the light curves of hot massive stars as discussed in §1, and thus it is unsurprising that it appears for these cooler stars. To model the red noise, we follow Blomme et al. (2011), and use the `curve_fit` routine in SciPy (Jones et al. 2001–) to fit the Lomb-Scargle periodogram with the function

$$\alpha(f) = \frac{\alpha_0}{1 + (2\pi\tau f)^\gamma} + \alpha_w \tag{5}$$

from Stanishev et al. (2002), where f is the frequency, α_0 is the power as $f \to 0$, tau is a characteristic timescale, and α_w is an additional parameter we add in to model the white noise floor at the highest frequencies (ostensibly equal to the instrumental noise). We perform this

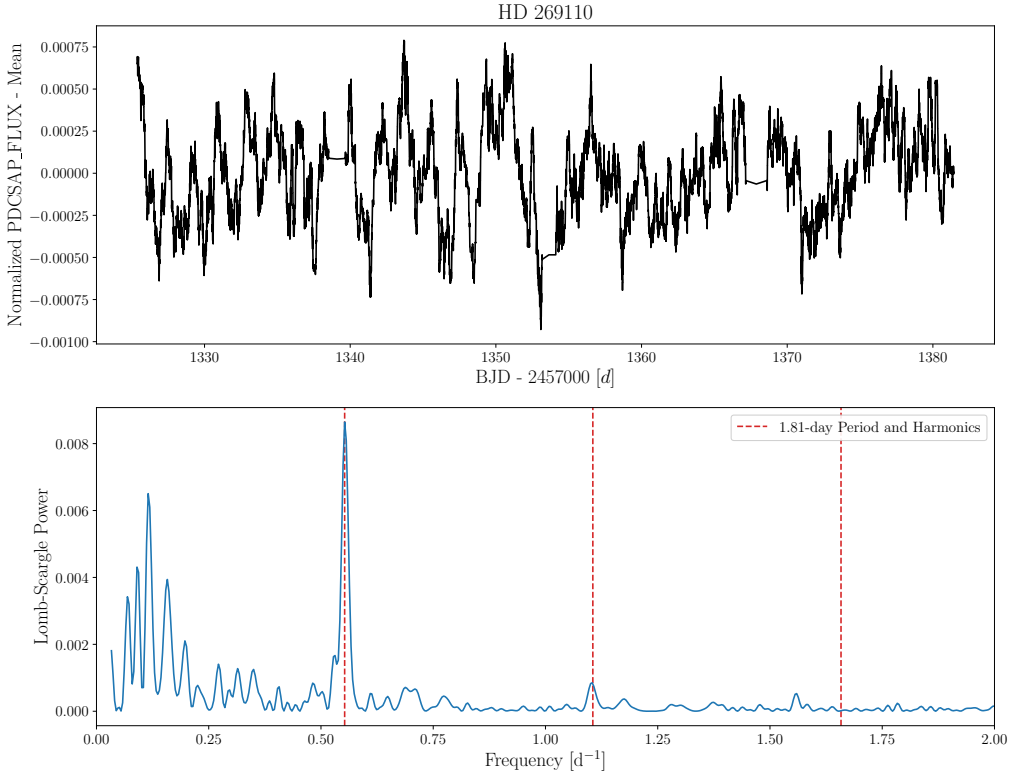

Figure 4. Similar to Figure 3, for HD 269110.

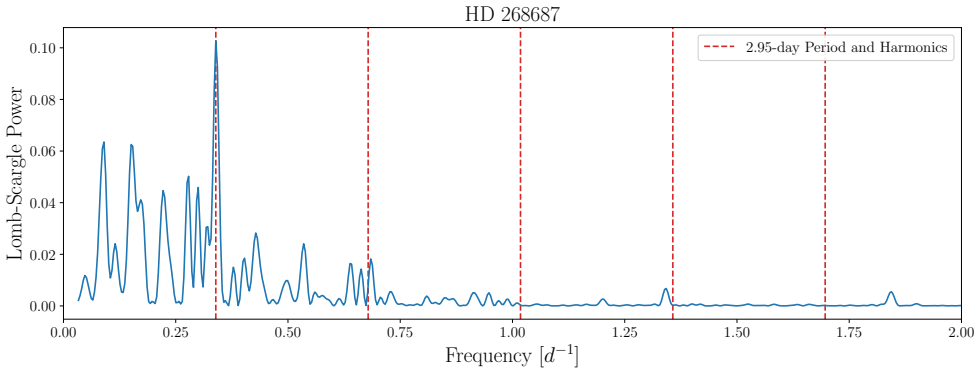

Figure 5. Periodogram for HD 268687, showing a clear peak corresponding to a period of 2.95 days. We indicate this frequency and its first four harmonics with vertical red lines.

fit after calculating the base-10 logarithm of both the Lomb-Scargle power and the fitting function to avoid artificial weighting of real peaks at high frequencies.

The periodograms and fits for all five YSGs are shown in Figure 6. It is immediately clear that the noise characteristics of all of the light curves differ, indicating that the source of the noise is likely astrophysical. The parameter values and 1σ error estimates are compiled in Table 2, and compared to the physical properties of the stars. HD 269953 is quantitatively different from the other YSGs in all parameters but the white noise component of the fit. Notably the red noise power-law component of the fit is only readily apparent over a narrow range of frequencies $\sim 2 - 4$ day^{-1}, but the power law

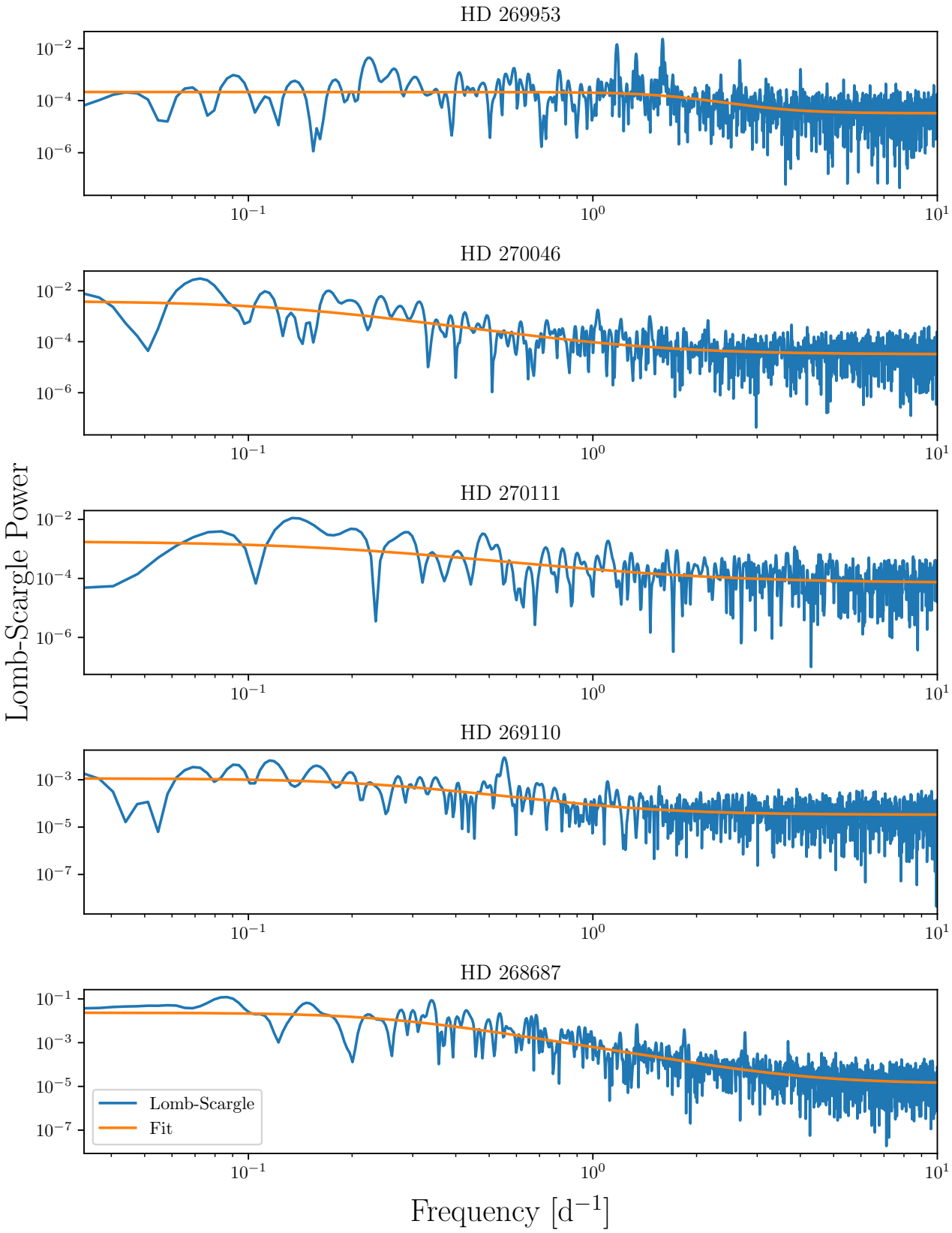

Figure 6. Lomb-Scargle periodograms calculated between 1/30 and 10 day^{-1} for all five YSGs. Fits using equation (5) are in orange.

slope is approximately twice as steep as the four other YSGs. Combined with its status as the dustiest YSG in the sample, it is clear that this object warrants further follow-up in the short-timescale regime. Finally, both of the F supergiants have significantly higher power at the lowest frequencies (α_0). With a larger sample of YSGs, comparisons between physical quantities and noise parameters will help constrain the origin of this noise, which has not been detected until now.

3.2. *Luminous Blue Variables*

Arguably one of the least understood stellar evolutionary phases, luminous blue variables (LBVs) are a phenomenological class consisting of extremely luminous stars that show signs of dramatic variability. LBVs are perhaps best characterized by their giant eruptions (such as those famously associated with η Carina and P Cygni), bright enough to be mistaken as supernovae. In some cases these "impostor" events are followed by true supernovae on timescales of a few years, as in the case of SN 2009ip, which underwent two outbursts in 2009 and 2010 before potentially undergoing a terminal explosion in 2012, e.g. (Mauerhan et al. 2013; Fraser et al. 2015). However, LBVs also experience large episodic variations in their effective temperatures on timescales of months to years, known as "S Dor variations". With their bolometric luminosities remaining almost constant, these S Dor variations manifest as horizontal evolution on the Hertzsprung-Russell diagram between their hot and cool states. LBVs also exhibit ∼0.1 mag irregular microvariability on timescales of weeks to months (Abolmasov 2011).

The evolutionary state of LBVs, their status as single or binary stars, and the physical mechanisms driving the S Dor variations are all topics of current debate (see Smith & Tombleson 2015; Humphreys et al. 2016; Aadland et al. 2018, Levesque & Lamers 2019). One possibility is that pulsations may be important for driving mass loss for S Doradus variability (Lovekin & Guzik 2014), and may therefore be observable. Indeed, a simple estimate of the dynamical/free-fall timescale for a typical LBV from Abolmasov (2011) yields

$$t_{dyn} \approx 0.6 \left(\frac{R_*}{10^{12} \mathrm{cm}} \right)^{3/2} \left(\frac{M_*}{100 \mathrm{M}_\odot} \right)^{-1/2} \mathrm{d} \qquad (6)$$

and variability on this timescale is easily observable by TESS. However, LBVs tend to be surrounded by a complex and sometimes dusty CSM — indeed, both LBVs studied here have incredibly red colors in Table 1 — so these pulsations may be attenuated and modulated by this intervening material. All told, understanding the short timescale variability of LBVs can offer incredibly valuable insight into the physical state of LBVs and their immediate environments.

3.2.1. *HD 269582*

HD (sometimes HDE) 269582 was observed as a H-rich Ofpe/WN9 or WN10h Wolf-Rayet star as recently as the mid 1990s (Crowther & Smith 1997). However, since 2003, it has entered an outbursting LBV state, rapidly brightening in V-band as it cooled to a late-B/early-A spectral type, accompanied by drastic changes in various line profiles (Walborn et al. 2017). Because HD 269582 appears to be newly entering the LBV phase, studying its variability can be quite instructive. Indeed, a link between light curve structure and outbursts has been proposed for Be stars (Huat et al. 2009; Kurtz et al. 2015); such a link for LBVs may even be testable with an entire year of observations.

The light curve for HD 269582 presented in the third panel of Figure 2 shows coherent ∼1%-level variability on timescales of a few days. The periodogram shown in Figure 7 shows a strong peak at 0.201 days^{-1} (corresponding to a 4.97-day period) with small peaks to either side. Though TESS only observed HD 269582 for 5 full cycles of this measured period, the shape of the light curve from cycle to cycle changes noticeably. This can be seen in the dynamic plot in Figure 8, showing the flux as a function of phase from cycle to cycle. The phase of maximum luminosity appears to shift from cycle to cycle, while the amplitude of modulation decreases.

Similar periods and changes in the light curve shape were observed in WR 110 by Chené et al. (2011). The 30-day light curve presented there appears remarkably similar to the TESS light curve of HD 269582. Chené et al. (2011) attributed the behavior of WR 110 to CIR in the wind, implying that we are measuring the rotational frequency. It is also possible that this frequency and the surrounding peaks in the periodogram are nonradial pulsations. Longer monitoring by TESS will enable us to resolve these peaks further, and build a more physical model with well-sampled parameter distributions, and spectroscopic monitoring would allow us to confirm a CIR scenario.

3.2.2. *S Doradus*

S Doradus is the prototypical S Dor variable, with a long history of photometric and spectroscopic observations. van Genderen et al. (1997) detected a ∼7 year period in S Dor's light curve, which Abolmasov (2011) argued is more likely to be a timescale associated with the duration of individual flaring events.

The light curve presented in Figure 2 shows strong ∼1% variations on sub-day timescales. The periodogram (Figure 9 shows a series of strong peaks be-

Table 2. Summary of the fit results to the periodograms of the five YSGs in our sample, along with their physical properties when available from Neugent et al. (2012)..

Common Name	Literature Spectral Type	$\log(L/L_\odot)$	T_{eff}/K	$\alpha_0/10^{-4}$	$\tau/10^{-2}$d	γ	$\alpha_w/10^{-5}$
HD 269953	G0 0 (Keenan & McNeil 1989)	5.437	4920	1.82 ± 0.18	8.33 ± 0.63	3.99 ± 0.61	3.26 ± 0.15
HD 270046	F8Ia (Ardeberg et al. 1972)	—	—	39.17 ± 14.39	123.98 ± 36.82	2.00 ± 0.15	3.23 ± 0.12
HD 270111	G5I (Sanduleak 1970)	—	—	17.51 ± 8.93	79.42 ± 48.63	1.55 ± 0.30	7.10 ± 0.65
HD 269110	G0I (Ardeberg et al. 1972)	5.251	5624	11.09 ± 2.91	63.50 ± 15.22	2.16 ± 0.23	3.34 ± 0.13
HD 268687	F6Ia (Ardeberg et al. 1972)	5.169	6081	234.24 ± 49.69	63.25 ± 7.79	2.63 ± 0.09	1.35 ± 0.08

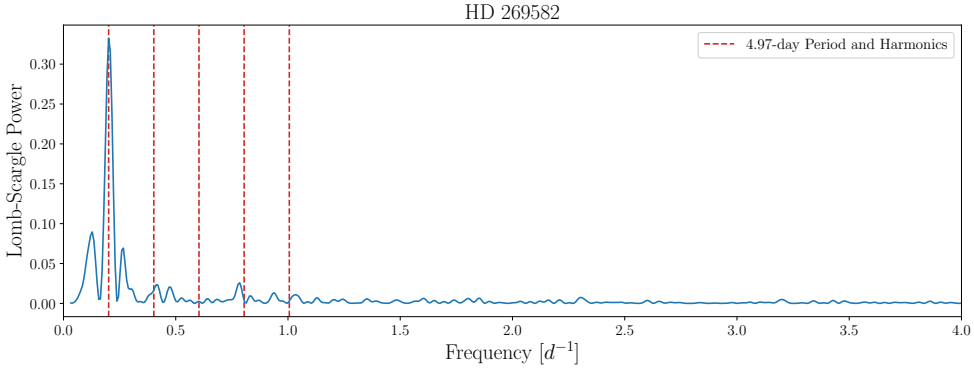

Figure 7. Periodogram for HD 269582, showing a clear peak corresponding to a period of 4.97 days. We indicate this frequency and its first four harmonics with vertical red lines.

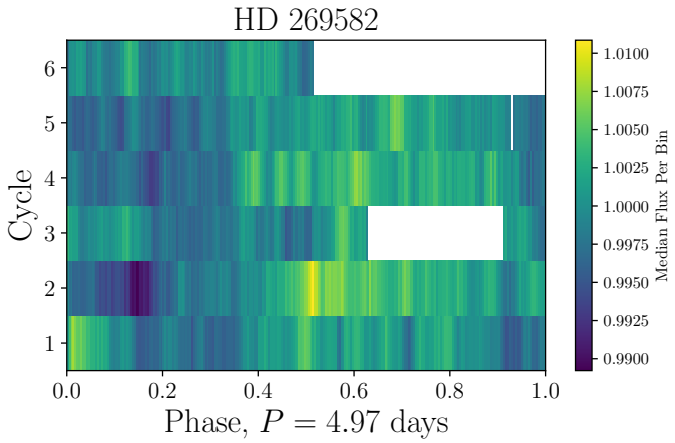

Figure 8. Dynamic plot, phased to a 4.97-day period for HD 269582, showing the variability from cycle to cycle.

low 1.5 day^{-1}, the two strongest of which are at 0.18 and 0.74 day^{-1} (periods of 5.58 and 1.35 days) respectively. These appear to be consistent with the time between large and small peaks in the light curve respectively. This may be indicative of the two periods beating against each other. While the lower frequency component appears to display some harmonics in the periodogram (shown by the vertical red lines), the higher frequency component (shown by the vertical purple lines) does not, and a number of other peaks in the periodogram do not appear to be associated with either frequency. Due to the lack of any single dominant signal, the complexity in the periodogram, and the current theoretical debate on the physical origin of S Dor outbursts, we reserve further modelling until a longer baseline TESS light curve is available, in the hopes of measuring lower frequencies, and resolving the periodogram peaks better.

3.2.3. *LBV Noise Properties*

In addition to our search for coherent variability in the two LBVs, we also analyze the noise properties of their light curves, using Equation 5 to fit the (log of the) Lomb-Scargle periodograms between 1/30 and 10 day^{-1}. The resulting fit parameters are presented in Table 3, and the fits themselves are shown in Figure 10.

In HD 269582, the power-law component dominates at most timescales, with the red noise power far exceeding the white noise, as indicated by the negative value of α_w. When we force all parameters to have values ≥ 0, we find that α_0 and τ decrease by a factor of ~ 2, while γ increases to 2.22. In S Dor, the power law slope is far steeper $\gamma = 3.73$. In longer-cadence AAVSO data, Abolmasov (2011) fit the power spectra with a

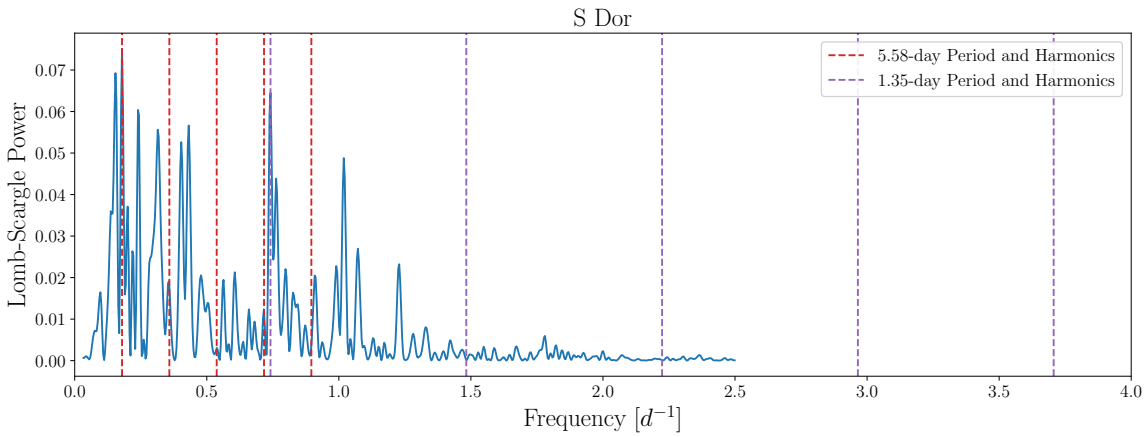

Figure 9. Periodogram for S Dor, calculated between 1/30 and 2.5 day^{-1}.

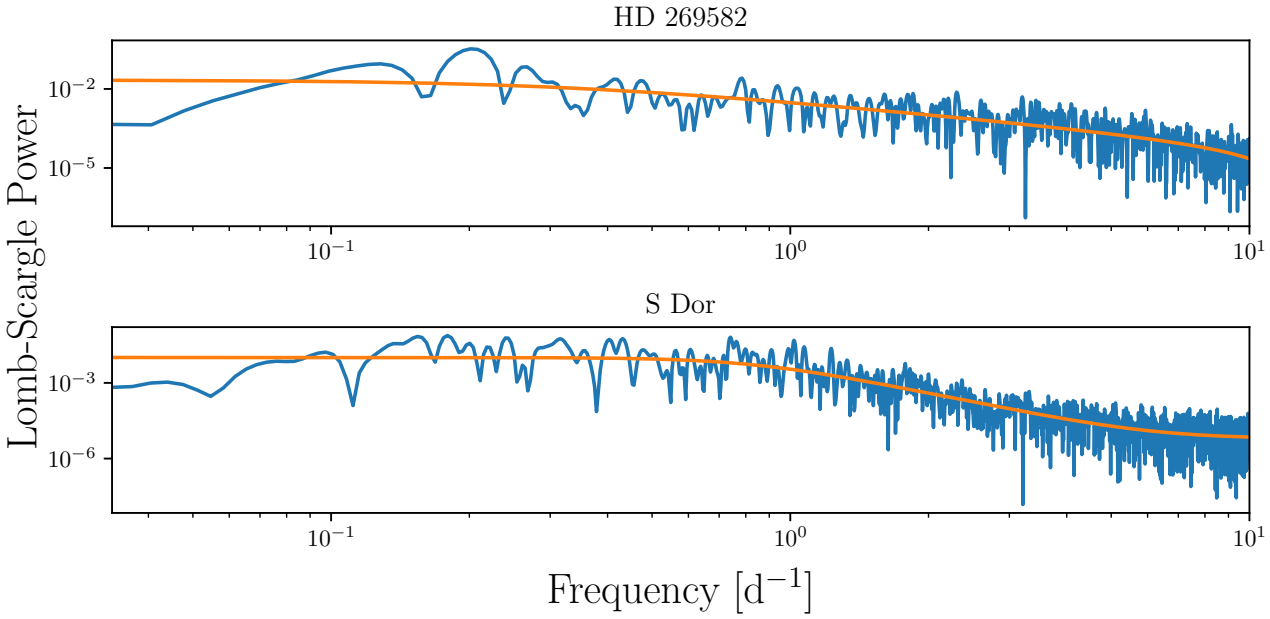

Figure 10. Lomb-Scargle periodograms calculated between 1/30 and 10 day^{-1} for both LBVs. Fits using equation (5) are in orange.

pure power law model, and found slopes closer to 2 for strongly flaring objects, and flatter slopes for LBVs in quiescence. While the TESS data don't probe the low-frequency regime measured by Abolmasov (2011), they do indicate that, in S Dor, the color of the stochastic noise in the light curves changes at higher frequency, while in HD 269582, the color of the noise remains consistent. This suggests that the variability on sub-day timescales in LBVs may be generated by a mixture of physical processes.

Table 3. Summary of the fit results to the periodograms of the two LBVs in our sample..

Common Name	$\alpha_0/10^{-4}$	$\tau/10^{-2}$d	γ	$\alpha_w/10^{-5}$
HD 269582	218.17 ± 64.89	47.94 ± 14.01	1.64 ± 0.11	-5.92 ± 1.48
S Dor	101.59 ± 10.32	18.94 ± 0.96	3.73 ± 0.10	0.61 ± 0.05

4. DISCUSSION

From this small sample of stars it is impossible to make many sweeping inferences. However, the broad range of light curve characteristics, unexpected characteristic time scales, and the structured noise properties

displayed by almost every star in this sample make it clear that rare, evolved massive stars are prime candidates for study with TESS and subsequent missions.

Of the light curves that display clear periodicity, only one (the LBV HD 269582) appears to be on a timescale that could be consistent with a rotational period. Rotation is a deeply important parameter for massive stars which can have drastic effects on their evolution (Ekström et al. 2012). Current samples of measured rotation periods in massive stars are insufficient to statistically measure the distribution of rotation rates, leaving us with spectroscopic measurements (e.g., Huang et al. 2010) which are hindered by the unknown inclination of the star relative to the line of sight. *Kepler* has revolutionized the study of stellar rotation for low-mass (FGKM) stars, increasing the known sample from $\sim 10^3$ to over 30,000. Comparison between physical properties and observed rotation periods for low-mass stars from *Kepler* has yielded new insights about magnetic braking evolution and potentially the age distribution of nearby stars in our Galaxy (e.g. van Saders et al. 2016; Davenport & Covey 2018).

None of the light curves we study display a clear signature of binary interactions. Binary interactions are critical in determining the evolution of many (if not most) massive stars. Galactic O stars have an intrinsic binary fraction of at least $\sim 70\%$ (Sana et al. 2012), while the binary fraction in the lower-metallicity LMC appears to be lower (Sana et al. 2013; Dorn-Wallenstein & Levesque 2018). Many of the physics governing these interactions can be constrained by observing post-main-sequence massive stars in binary systems. Unfortunately, very few such systems are known: the observed Wolf-Rayet binary fraction is $\sim$30% (Neugent & Massey 2014), while the binary fraction of yellow and red supergiants is still unknown (Levesque 2017). It is difficult to reconcile these low numbers with the high binary fraction of main sequence stars. Between the complex circumstellar geometry, and the already-complicated spectra of evolved massive stars, the detection of binary systems via radial velocity measurements is arduous. Photometric diagnostics can be used to find candidate RSG+B systems (Neugent et al. 2018), but for many other configurations, photometric variability may be one of the few detectable signatures of binary effects. These variations may manifest themselves as eclipses in well-aligned systems, ellipsoidal variations in short-period systems, or periodic outbursts in extremely eccentric systems as the system approaches periastron. Detecting these effects with TESS and characterizing binary systems with follow-up observations is a critical first step in understanding late-stage massive binary evolution, and resolving the discrepancy between the statistics of main sequence and evolved massive binaries.

Stars with periodicities inconsistent with rotation or binary interactions possess variability on timescales consistent with asteroseismic pulsations. Pulsational modes can give us deep insight into fundamental stellar properties like mass and radius. However, current asteroseismic models often rely upon scaling relations based on the sun (Kjeldsen & Bedding 1995). While stretching these scaling relations to stars like red giants is possible via some modifications (Gaulme et al. 2016), the interiors of evolved massive stars aren't analogous to the sun in the slightest. Developing suitable models will allow us to constrain the interior structures of massive stars, and understand energy transport at an unprecedented level. The impact of wave-energy deposition in the last century of a massive star's life can have important impacts on its pre-supernova evolution (Fuller 2017), and measuring the pulsational properties of the most massive stars will give us valuable constraints on the masses of supernova progenitors.

Finally, red noise is a ubiquitous property in all of the light curves. Whether this noise arises from decoherent asteroseismic pulsations, surface granulations in the cooler stars, wind instabilities in the hot stars, or some other process entirely, measuring the noise characteristics of a large sample of massive stars will allow us to search for trends as a function of evolutionary stage, which can give us some insight into the physical processes involved. All told, studying evolved massive stars at short timescales can help us answer many unsolved problems in massive star evolution.

5. SUMMARY & CONCLUSION

Our main results are summarized as follows:

- We study seven evolved massive stars. We find distinct periodicity in five stars, including two luminous blue variables, and three yellow supergiants. We are unable to constrain the source of the variability in all cases.

- The light curve of one YSG, HD 269953, displays unique properties not shared by its fellow YSGs. We suggest that it is in a post-RSG evolutionary phase.

- All of the YSGs display red noise in their light curves, that is likely astrophysical in origin.

- The LBV HD 269582 displays 1% variability at $\sim$5 day timescales. While the shape of the variability changes, it is possibly due to a rotation period that

is imprinting itself into the wind of HD 269582 via a co-rotating interaction region.

- S Doradus exhibits incredible complexity in its peridogram at frequencies below ~ 1.5 day^{-1}, including two seemingly dominant periods at 1.35 and 5.58 that appear to be beating against each other.

- Both LBVs display red noise. A shallow power-law component dominates in HD 269582, S Dor displays a very steep power law at high frequencies, before flattening at lower frequencies.

We wish to emphasize that evolved massive stars have never been studied before with high cadence space based photometry. As the observed baseline increases for stars in the TESS sourthern CVZ, the periodogram peaks will grow sharper, and allow us to probe lower frequencies for comparison with previous studies. However, our tentative results presented here highlight the importance of studying massive stars in this domain. It is clear that new models are required to explain the observed variability, which will allow these data to give us an incredibly deep insight into the physics of evolved massive stars.

This work was supported by NSF grant AST 1714285 awarded to E.M.L.

JRAD acknowledges support from the DIRAC Institute in the Department of Astronomy at the University of Washington. The DIRAC Institute is supported through generous gifts from the Charles and Lisa Simonyi Fund for Arts and Sciences, and the Washington Research Foundation

This work made use of the following software:

Software: Astropy v3.0.4 (Astropy Collaboration et al. 2013; The Astropy Collaboration et al. 2018), Matplotlib v2.2.2 (Hunter 2007), makecite v0.4 (Price-Whelan et al. 2018), NumPy v1.15.2 (Van Der Walt et al. 2011), Pandas v0.23.4 (McKinney 2010), Python 3.5.1, SciPy v1.1.0 (Jones et al. 2001–)

REFERENCES

Aadland, E., Massey, P., Neugent, K. F., & Drout, M. R. 2018, AJ, 156, 294, doi: 10.3847/1538-3881/aaeb96

Abolmasov, P. 2011, NewA, 16, 421, doi: 10.1016/j.newast.2011.03.006

Ardeberg, A., Brunet, J. P., Maurice, E., & Prevot, L. 1972, Astronomy and Astrophysics Supplement Series, 6, 249

Arellano Ferro, A. 1985, MNRAS, 216, 571, doi: 10.1093/mnras/216.3.571

Astropy Collaboration, Robitaille, T. P., Tollerud, E. J., et al. 2013, A&A, 558, A33, doi: 10.1051/0004-6361/201322068

Bailer-Jones, C. A. L., Rybizki, J., Fouesneau, M., Mantelet, G., & Andrae, R. 2018, AJ, 156, 58, doi: 10.3847/1538-3881/aacb21

Balona, L. A. 2016, MNRAS, 457, 3724, doi: 10.1093/mnras/stw244

Balona, L. A., Baran, A. S., Daszyńska-Daszkiewicz, J., & De Cat, P. 2015, MNRAS, 451, 1445, doi: 10.1093/mnras/stv1017

Balona, L. A., Pigulski, A., De Cat, P., et al. 2011, MNRAS, 413, 2403, doi: 10.1111/j.1365-2966.2011.18311.x

Blomme, R., Mahy, L., Catala, C., et al. 2011, A&A, 533, A4, doi: 10.1051/0004-6361/201116949

Bonanos, A. Z., Massa, D. L., Sewilo, M., et al. 2009, AJ, 138, 1003, doi: 10.1088/0004-6256/138/4/1003

Buysschaert, B., Aerts, C., Bloemen, S., et al. 2015, MNRAS, 453, 89, doi: 10.1093/mnras/stv1572

Chené, A. N., Moffat, A. F. J., Cameron, C., et al. 2011, ApJ, 735, 34, doi: 10.1088/0004-637X/735/1/34

Chiavassa, A., Pasquato, E., Jorissen, A., et al. 2011, A&A, 528, A120, doi: 10.1051/0004-6361/201015768

Choi, J., Dotter, A., Conroy, C., et al. 2016, ApJ, 823, 102, doi: 10.3847/0004-637X/823/2/102

Cranmer, S. R., & Owocki, S. P. 1996, ApJ, 462, 469, doi: 10.1086/177166

Crowther, P. A., & Smith, L. J. 1997, A&A, 320, 500

Cutri, R. M., Skrutskie, M. F., van Dyk, S., et al. 2003, VizieR Online Data Catalog, 2246

Daszynska-Daszkiewicz, J., Walczak, P., Szewczuk, W., & Pamyatnykh, A. 2018, ArXiv e-prints. https://arxiv.org/abs/1812.00075

Davenport, J. R. A., & Covey, K. R. 2018, ApJ, 868, 151

Dorn-Wallenstein, T. Z., & Levesque, E. M. 2018, ArXiv e-prints. https://arxiv.org/abs/1810.01902

Dotter, A. 2016, ApJS, 222, 8, doi: 10.3847/0067-0049/222/1/8

Ekström, S., Georgy, C., Eggenberger, P., et al. 2012, A&A, 537, A146, doi: 10.1051/0004-6361/201117751

Fraser, M., Kotak, R., Pastorello, A., et al. 2015, MNRAS, 453, 3886, doi: 10.1093/mnras/stv1919

Fuller, J. 2017, MNRAS, 470, 1642, doi: 10.1093/mnras/stx1314

Gaia Collaboration, Brown, A. G. A., Vallenari, A., et al. 2018, A&A, 616, A1, doi: 10.1051/0004-6361/201833051

Garcia-Segura, G., Langer, N., & Mac Low, M.-M. 1996, A&A, 316, 133

Gaulme, P., McKeever, J., Jackiewicz, J., et al. 2016, ApJ, 832, 121, doi: 10.3847/0004-637X/832/2/121

Gordon, K. D., Clayton, G. C., Misselt, K. A., Landolt, A. U., & Wolff, M. J. 2003, ApJ, 594, 279, doi: 10.1086/376774

Gvaramadze, V. V., Kniazev, A. Y., Castro, N., & Grebel, E. K. 2018, ArXiv e-prints. https://arxiv.org/abs/1812.00007

Habets, G. M. H. J., & Heintze, J. R. W. 1981, A&AS, 46, 193

Huang, W., Gies, D. R., & McSwain, M. V. 2010, ApJ, 722, 605, doi: 10.1088/0004-637X/722/1/605

Huat, A.-L., Hubert, A.-M., Baudin, F., et al. 2009, A&A, 506, 95, doi: 10.1051/0004-6361/200911928

Humphreys, R. M., Weis, K., Davidson, K., & Gordon, M. S. 2016, ApJ, 825, 64, doi: 10.3847/0004-637X/825/1/64

Hunter, J. D. 2007, Computing In Science & Engineering, 9, 90

Johnston, C., Buysschaert, B., Tkachenko, A., Aerts, C., & Neiner, C. 2017, MNRAS, 469, L118, doi: 10.1093/mnrasl/slx060

Jones, E., Oliphant, T., Peterson, P., et al. 2001–, SciPy: Open source scientific tools for Python. http://www.scipy.org/

Keenan, P. C., & McNeil, R. C. 1989, The Astrophysical Journal Supplement Series, 71, 245, doi: 10.1086/191373

Kiss, L. L., Szabó, G. M., & Bedding, T. R. 2006, MNRAS, 372, 1721, doi: 10.1111/j.1365-2966.2006.10973.x

Kjeldsen, H., & Bedding, T. R. 1995, A&A, 293, 87

Kovács, G. 2000, A&A, 363, L1. https://arxiv.org/abs/astro-ph/0011056

Krtička, J., & Feldmeier, A. 2018, A&A, 617, A121, doi: 10.1051/0004-6361/201731614

Kurtz, D. W., Shibahashi, H., Murphy, S. J., Bedding, T. R., & Bowman, D. M. 2015, MNRAS, 450, 3015, doi: 10.1093/mnras/stv868

Levesque, E. M. 2017, Astrophysics of Red Supergiants (IOP Publishing Ltd.), doi: 10.1088/978-0-7503-1329-2

Lindegren, L., Hernández, J., Bombrun, A., et al. 2018, A&A, 616, A2, doi: 10.1051/0004-6361/201832727

Lomb, N. R. 1976, Ap&SS, 39, 447, doi: 10.1007/BF00648343

Lovekin, C. C., & Guzik, J. A. 2014, MNRAS, 445, 1766, doi: 10.1093/mnras/stu1899

Malhan, K., Ibata, R. A., & Martin, N. F. 2018, MNRAS, 481, 3442, doi: 10.1093/mnras/sty2474

Massey, P. 2002, ApJS, 141, 81, doi: 10.1086/338286

Massey, P., Neugent, K. F., & Levesque, E. M. 2017, Philosophical Transactions of the Royal Society of London Series A, 375, 20160267, doi: 10.1098/rsta.2016.0267

Massey, P., Olsen, K. A. G., Hodge, P. W., et al. 2007, AJ, 133, 2393, doi: 10.1086/513319

Mauerhan, J. C., Smith, N., Filippenko, A. V., et al. 2013, MNRAS, 430, 1801, doi: 10.1093/mnras/stt009

McKinney, W. 2010, in Proceedings of the 9th Python in Science Conference, ed. S. van der Walt & J. Millman, 51 – 56

Moffat, A. F. J., St-Louis, N., Carlos-Leblanc, D., et al. 2018, in 3rd BRITE Science Conference, ed. G. A. Wade, D. Baade, J. A. Guzik, & R. Smolec, Vol. 8, 37–42

Mullan, D. J. 1984, ApJ, 283, 303, doi: 10.1086/162307

Neugent, K. F., Levesque, E. M., & Massey, P. 2018, AJ, 156, 225, doi: 10.3847/1538-3881/aae4e0

Neugent, K. F., & Massey, P. 2014, ApJ, 789, 10, doi: 10.1088/0004-637X/789/1/10

Neugent, K. F., Massey, P., Skiff, B., & Meynet, G. 2012, ApJ, 749, 177, doi: 10.1088/0004-637X/749/2/177

Papaloizou, J., & Pringle, J. E. 1978, Monthly Notices of the Royal Astronomical Society, 182, 423, doi: 10.1093/mnras/182.3.423

Paxton, B., Bildsten, L., Dotter, A., et al. 2011, ApJS, 192, 3, doi: 10.1088/0067-0049/192/1/3

Paxton, B., Cantiello, M., Arras, P., et al. 2013, ApJS, 208, 4, doi: 10.1088/0067-0049/208/1/4

Paxton, B., Marchant, P., Schwab, J., et al. 2015, ApJS, 220, 15, doi: 10.1088/0067-0049/220/1/15

Pedersen, M. G., Chowdhury, S., Johnston, C., et al. 2019, arXiv e-prints, arXiv:1901.07576. https://arxiv.org/abs/1901.07576

Perdang, J. 2009, in EAS Publications Series, Vol. 38, EAS Publications Series, ed. M. Goupil, Z. Koláth, N. Nardetto, & P. Kervella, 43–62

Price-Whelan, A., Mechev, A., & jumeroag. 2018, adrn/makecite: v0.1, doi: 10.5281/zenodo.1343295. https://doi.org/10.5281/zenodo.1343295

Puls, J., Vink, J. S., & Najarro, F. 2008, A&A Rv, 16, 209, doi: 10.1007/s00159-008-0015-8

Ramiaramanantsoa, T., Moffat, A. F. J., Harmon, R., et al. 2018, MNRAS, 473, 5532, doi: 10.1093/mnras/stx2671

Saio, H., Kurtz, D. W., Murphy, S. J., Antoci, V. L., & Lee, U. 2018, MNRAS, 474, 2774, doi: 10.1093/mnras/stx2962

Sana, H., de Mink, S. E., de Koter, A., et al. 2012, Science, 337, 444, doi: 10.1126/science.1223344

Sana, H., de Koter, A., de Mink, S. E., et al. 2013, A&A, 550, A107, doi: 10.1051/0004-6361/201219621

Sanduleak, N. 1970, Contributions from the Cerro Tololo Inter-American Observatory, 89

Scargle, J. D. 1982, ApJ, 263, 835, doi: 10.1086/160554

Smartt, S. J., Eldridge, J. J., Crockett, R. M., & Maund, J. R. 2009, MNRAS, 395, 1409, doi: 10.1111/j.1365-2966.2009.14506.x

Smith, N. 2014, ARA&A, 52, 487, doi: 10.1146/annurev-astro-081913-040025

Smith, N., & Tombleson, R. 2015, MNRAS, 447, 598, doi: 10.1093/mnras/stu2430

Stanishev, V., Kraicheva, Z., Boffin, H. M. J., & Genkov, V. 2002, A&A, 394, 625, doi: 10.1051/0004-6361:20021163

Stassun, K. G., Oelkers, R. J., Pepper, J., et al. 2018, AJ, 156, 102, doi: 10.3847/1538-3881/aad050

The Astropy Collaboration, Price-Whelan, A. M., Sipőcz, B. M., et al. 2018, ArXiv e-prints. https://arxiv.org/abs/1801.02634

Van Der Walt, S., Colbert, S. C., & Varoquaux, G. 2011, ArXiv e-prints, arXiv:1102.1523. https://arxiv.org/abs/1102.1523

van Genderen, A. M., Sterken, C., & de Groot, M. 1997, A&A, 318, 81

van Saders, J. L., Ceillier, T., Metcalfe, T. S., et al. 2016, Nature, 529, 181

Walborn, N. R., Gamen, R. C., Morrell, N. I., et al. 2017, AJ, 154, 15, doi: 10.3847/1538-3881/aa6195

Waters, L. B. F. M. 2010, in Astronomical Society of the Pacific Conference Series, Vol. 425, Hot and Cool: Bridging Gaps in Massive Star Evolution, ed. C. Leitherer, P. D. Bennett, P. W. Morris, & J. T. Van Loon, 267

Wood, P. R., Bessell, M. S., & Fox, M. W. 1983, ApJ, 272, 99, doi: 10.1086/161265

Yoon, S.-C., & Cantiello, M. 2010, ApJL, 717, L62, doi: 10.1088/2041-8205/717/1/L62